

Adaptive wavefront control using a nonlinear Zernike filter

Eric W. Justh^a, Mikhail A. Vorontsov^b, Gary W. Carhart^b, Leonid A. Beresnev^b, P.S. Krishnaprasad^a

^aInstitute for Systems Research & Dept. of Elect. and Comp. Eng., Univ. of Maryland, College Park

^bIntelligent Optics Laboratory, U.S. Army Research Lab, Adelphi, MD 20783

ABSTRACT

A conventional Zernike filter measures wavefront phase by superimposing the aberrated input beam with a phase-shifted version of its zero-order spectral component. The Fourier-domain phase-shifting is performed by a fixed phase-shifting dot on a glass slide in the focal plane of a Fourier-transforming lens. Using an optically-controlled phase spatial light modulator (SLM) instead of the fixed phase-shifting dot, we have simulated and experimentally demonstrated a nonlinear Zernike filter robust to wavefront tilt misalignments. In the experiments, a liquid-crystal light valve (LCLV) was used as the phase SLM. The terminology “nonlinear” Zernike filter refers to the nonlinear filtering that takes place in the Fourier domain due to the phase change for field spectral components being proportional to the spectral component intensities. Because the Zernike filter output intensity is directly related to input wavefront phase, a parallel, distributed feedback system can replace the wavefront reconstruction calculations normally required in adaptive-optic phase correction systems. Applications include high-resolution phase distortion suppression for atmospheric turbulence, optical phase microscopy, and compensation of aberrations in optical system components. A factor of eight improvement in Strehl ratio was obtained experimentally, and simulation results suggest that even better performance could be obtained by replacing the LCLV with a more sophisticated optically-controlled phase SLM.

Keywords: Zernike filter, adaptive optics, turbulence compensation, phase-contrast, wavefront sensing, phase measurement

1. INTRODUCTION

A conventional Zernike filter measures wavefront phase by superimposing the aberrated input beam with a phase-shifted version of its zero-order spectral component. The Fourier-domain phase-shifting is performed by a Zernike phase plate: a fixed phase-shifting dot on a glass slide in the focal plane of a Fourier-transforming lens. The superposition of the two parts of the beam with different spectral phase shifts produces an intensity pattern which, for small wavefront variations, is proportional to the wavefront. Using an optically controlled phase spatial light modulator (SLM) instead of the fixed phase-shifting dot, we have simulated and experimentally demonstrated a nonlinear Zernike filter robust to wavefront tilt misalignments. In the experiments we used a liquid-crystal light valve (LCLV) as the phase SLM. The LCLV device produces an optical phase shift distribution (for linearly polarized light having a certain axis of polarization) which is a function of the intensity distribution at the LCLV. The terminology “nonlinear” Zernike filter refers to the nonlinear filtering that takes place in the Fourier domain (due to the phase change for field spectral components being proportional to the spectral component intensities).

Because the Zernike filter output intensity is directly related to input wavefront phase, a parallel, distributed feedback system can replace the wavefront reconstruction calculations normally required in adaptive-optic phase correction systems. We have demonstrated (theoretically, in simulation, and by experiment) that the nonlinear Zernike filter can be used in a parallel, distributed feedback system with a phase-correcting SLM to perform high-resolution wavefront aberration correction. Adaptive optics applications include high-resolution phase distortion suppression for atmospheric turbulence, optical phase microscopy, and compensation of aberrations in optical system components.

First, the mathematical model and justification of the feedback control law are reviewed. Experimental results are then presented. With the nonlinear Zernike filter feedback system, we experimentally obtained a factor of eight improvement in Strehl ratio. Simulation results suggest that even better performance could be obtained by replacing the LCLV with a more sophisticated opto-electronic phase SLM.

2. NONLINEAR ZERNIKE FILTER FEEDBACK SYSTEM MODEL

2.1. Feedback controller synthesis

Consider the direct-control adaptive optics system shown in Fig. 1. This system consists of the following adaptive optics components: wavefront corrector, wavefront sensor, and feedback controller. All of the adaptive system components are assumed to have high spatial resolution, and thus a continuously distributed approximation of the adaptive system model can be used. The wavefront corrector introduces a phase modulation $u(\mathbf{r},t)$ into the distorted input wave $A_{in}(\mathbf{r},t) = A_0(\mathbf{r}) \exp[i\varphi(\mathbf{r},t)]$. The corrected wave $A_{cor}(\mathbf{r},t) = A_0(\mathbf{r}) \exp\{i[\varphi(\mathbf{r},t) + u(\mathbf{r},t)]\}$ is used as the wavefront sensor input. The wavefront sensor is interfaced with the feedback controller. In comparison with conventional adaptive optics architectures, the phase reconstructor is absent and the feedback controller operates directly using the sensor's output intensity $I_{out}(\mathbf{r},t)$.

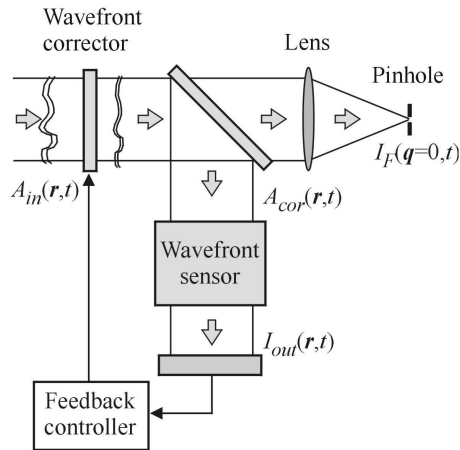


Fig. 1. Schematic of a direct-control adaptive optics system.

The dependence of the correction function u on the wavefront sensor output I_{out} defines the control algorithm built into the feedback controller. For a continuous time controller, this algorithm can be represented as a time-dependent controlling-phase evolution process:

$$\frac{\partial u(\mathbf{r},t)}{\partial t} = G[u, I_{out}], \quad (1)$$

where G is an operator describing the feedback controller. Synthesis of the wavefront controller G can be based on different principles. In the diffractive feedback adaptive system, both the wavefront sensor and the controller G are selected based on an analysis of the nonlinear spatio-temporal dynamics (1).^{1,2} The major requirement for these dynamics, or equivalently for the feedback controller design, is the existence of stationary state solutions of (1) corresponding to phase distortion suppression.

Another approach for wavefront controller synthesis is based on the gradient optimization technique.³⁻⁵ In this case the control rule (1) describes a continuous-time gradient-descent optimization of a system performance metric J :

$$\frac{\partial u(\mathbf{r},t)}{\partial t} = \eta J'(\mathbf{r},t), \quad (2)$$

where $J'(\mathbf{r},t)$ is a first variation (gradient) of the cost functional and η is a constant positive for cost functional maximization and negative otherwise. There are two approaches that can be used for practical implementation of the gradient descent algorithm (2): model-free, and gradient-flow optimization. In the model-free optimization technique, an approximation $\tilde{J}'(\mathbf{r},t)$ is used instead of the "true" gradient $J'(\mathbf{r},t)$. This approximation can be obtained by applying a small perturbation δu to the wavefront corrector and measuring the corresponding change δJ of the system performance metric. For the case of the recently developed parallel stochastic gradient descent technique, the gradient approximation used is proportional to the product $\delta J \delta u$.⁶⁻⁹ The relatively low convergence rate is the major drawback of the model-free optimization technique, particularly noticeable for high-resolution adaptive optics.

A different idea is utilized in the gradient-flow optimization method, which is widely used for digital image processing applications.¹⁰⁻¹² The gradient $J'(\mathbf{r},t)$ is calculated analytically based on knowledge of the system's mathematical model and performance metric. The problem is that in most adaptive optics applications, the system model, which includes phase aberrations, is unknown. In addition, for practical implementation of the gradient-flow technique in adaptive optics, the gradient $J'(\mathbf{r},t)$ should be dependent only on available information: here, the wavefront sensor output intensity $I_{out}(\mathbf{r},t)$ and the controlling phase $u(\mathbf{r},t)$. This requires gradient representation in the following form: $J'(\mathbf{r},t) = J'[u, I_{out}]$. The nonlinear Zernike filter feedback system we use is related to a gradient-flow direct-control technique (in the sense that the dynamics include a gradient-flow term, along with other terms that disappear when the system is linearized).

2.2. System performance metric and gradient-flow dynamics

For a number of adaptive optics applications, a natural measure of system performance in correcting the aberrated wavefront is the Strehl ratio $St = I_F(q=0)/I_F^0$. Here $I_F(q)$ is the intensity of the output wave in the lens focal plane (Fig. 1), and I_F^0 is the corresponding intensity in the absence of phase aberrations. Maximization of the Strehl ratio using the gradient descent technique may result in two undesirable phenomena: drift of the aperture-averaged phase $\bar{u}(t)$ towards the edge of the wavefront corrector operational range, and phase discontinuities, both of which may occur during the adaptation process. To prevent aperture-averaged phase drift and to smooth the controlling phase (i.e., to suppress discontinuities and noise) the system performance metric J may include (besides the Strehl ratio) additional penalty terms:

$$J[u] = St - \alpha_1 [\bar{u}(t) - u_0]^2 - \alpha_2 \int |\nabla u(\mathbf{r},t)|^2 d^2\mathbf{r}, \quad (3)$$

where $\bar{u}(t) = S^{-1} \int u(\mathbf{r},t) d^2\mathbf{r}$ is the aperture-averaged phase, u_0 is a desirable value for $\bar{u}(t)$, and α_1 and α_2 are weight coefficients determining penalty term contributions. For now, ignore in (3) the time dependence of both phase aberrations and the controlling phase by assuming that phase aberrations are stationary state ("frozen"). The complex amplitude of the input field (after passing through the wavefront corrector) can then be represented in the form $A_{cor}(\mathbf{r}) = A_0(\mathbf{r}) \exp\{i[u(\mathbf{r}) + \tilde{\varphi}(\mathbf{r})]\}$. Equation (3) then becomes

$$J[u] = \left| \int A_0(\mathbf{r}) \exp\{i[u(\mathbf{r}) + \tilde{\varphi}(\mathbf{r})]\} d^2\mathbf{r} \right|^2 - \beta_1 [u_0 - S^{-1} \int u(\mathbf{r}) d^2\mathbf{r}]^2 - \beta_2 \int |\nabla u(\mathbf{r})|^2 d^2\mathbf{r}, \quad (4)$$

where $\tilde{\varphi}(\mathbf{r}) = \varphi(\mathbf{r}) - \bar{\varphi}$ is the spatially modulated component of the wavefront aberration, and β_1 and β_2 are new weight coefficients. The first term in (4) is proportional to the intensity of the input field zero spectral component $I_F(q=0)$. Note that expressions for the weighting coefficients in (4) are irrelevant for the analysis below and for this reason are not defined. Consider the variation δJ of the cost functional resulting from the small perturbation δu of the controlling phase:

$$\delta J = J[u + \delta u] - J[u] = \int J'(\mathbf{r}) \delta u(\mathbf{r}) d^2\mathbf{r} + o(\delta u), \quad (5)$$

where the term $o(\delta u)$ describes second and higher order terms with respect to the phase variation δu . Using (5) for the cost functional gradient we obtain

$$J' = -2 \bar{A}_0 |A_0(\mathbf{r}) \sin[u(\mathbf{r}) + \tilde{\varphi}(\mathbf{r}) - \Delta] - 2\beta_1 (\bar{u} - u_0) + 2\beta_2 \nabla^2 u(\mathbf{r}), \quad (6)$$

where $\bar{A}_0 \equiv \left| \bar{A}_0 \right| \exp(i\Delta) = \int A_0(\mathbf{r}) \exp\{i[u(\mathbf{r}) + \tilde{\varphi}(\mathbf{r})]\} d^2\mathbf{r}$.¹³ Note that the value $\left| \bar{A}_0 \right|^2$ in (6) is proportional to the Strehl ratio.

If we now embed the control function $u(\mathbf{r})$ in a family of time-dependent functions $u(\mathbf{r},t)$ and consider the time-dependent evolution of J in the direction of the cost functional gradient, the gradient-flow dynamics (2) thus leads to the following nonlinear diffusion equation describing the controlling phase update:

$$\frac{\partial u(\mathbf{r},t)}{\partial t} = d \nabla^2 u(\mathbf{r},t) - \gamma \bar{A}_0(t) |A_0(\mathbf{r}) \sin[u(\mathbf{r},t) + \tilde{\varphi}(\mathbf{r}) - \Delta] - \mu [\bar{u}(t) - u_0]. \quad (7)$$

The coefficients d , γ and μ are dependent on the parameters α_1 , α_2 , and η introduced in (2) and (3).

2.3. Conventional Zernike filter output intensity

The schematic for a conventional wavefront sensor based on the Zernike phase contrast technique (Zernike filter) is shown in Fig. 2. It consists of two lenses with a phase-changing plate (Zernike phase plate) placed in the lenses' common focal plane. The phase plate has a small circular region (a dot) in the middle that introduces a phase shift θ near $\pi/2$ radians into the focused wave.^{14,15} The radius of the dot, a_F , is typically chosen to equal the diffraction-limited radius a_F^{dif} of a focused, undistorted input wave. The complex transfer function $T(\mathbf{q})$ for the focal-plane filter is

$$\begin{aligned} T(\mathbf{q}) &= e^{i\theta} \text{ for } |\mathbf{q}| \leq q_0, \text{ and} \\ T(\mathbf{q}) &= 1 \text{ otherwise.} \end{aligned} \quad (8)$$

The wave vector \mathbf{q} is associated with the focal plane radial vector \mathbf{r}_F through $\mathbf{q} = \mathbf{r}_F / (\lambda F)$, where F is the lens focal length, λ is wavelength, and $q_0 = a_F / (\lambda F)$ is the cutoff frequency corresponding to the dot size a_F . For the sake of convenience, consider the following variable normalization: the radial vectors \mathbf{r} in the sensor input/output plane and \mathbf{r}_F in the focal plane are normalized by lens aperture radius a , the wave vector \mathbf{q} by a^{-1} , and the lens focal length by the diffraction parameter ka^2 (where $k = 2\pi/\lambda$ is the wave number). Correspondingly, in the normalized variables, $\mathbf{q} = \mathbf{r}_F / (2\pi F)$ and $q_0 = a_F / (2\pi F)$ (where the dot size a_F is also normalized by a).

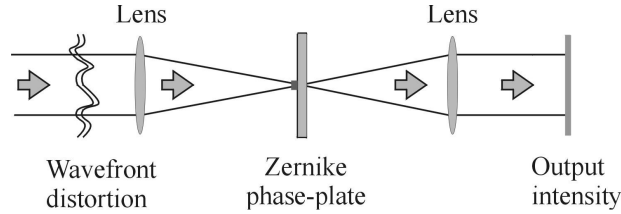


Fig. 2. Conventional Zernike filter.

Consider a simplified model corresponding to a focal plane filter affecting only the zero-spectral component. In this case we have $T(\mathbf{0}) = e^{i\theta}$ and $T(\mathbf{q}) = 1$ for $\mathbf{q} \neq \mathbf{0}$. Assume an input wave $A_{in}(\mathbf{r}) = A_0(\mathbf{r}) \exp[i\phi(\mathbf{r})]$ enters a wavefront sensor, where $I_0(\mathbf{r}) = A_0^2(\mathbf{r})$ and $\phi(\mathbf{r})$ are the input wave intensity and phase spatial distributions. The sensor's front lens performs a Fourier transform of the input wave. Within the accuracy of a phase factor, $A(\mathbf{q}) = (2\pi F)^{-1} F[A_{in}(\mathbf{r})]$, where $F[\]$ is the Fourier transform operator and $A(\mathbf{q})$ is the spatial spectral amplitude of the input field (i.e., the field complex amplitude in the focal plane).¹⁵ In normalized variables, the field intensity in the focal plane can be expressed as a function of spatial frequency: $I_F(\mathbf{q}) = (2\pi F)^{-2} |A(\mathbf{q})|^2$. The influence of the focal plane filter can be accounted for by multiplying $A(\mathbf{q})$ by the transfer function $T(\mathbf{q})$:

$$A_{out}(\mathbf{q}) = A(\mathbf{q})[1 - \delta(\mathbf{q})] + e^{i\theta} A(\mathbf{q})\delta(\mathbf{q}), \quad (9)$$

where $A_{out}(\mathbf{q})$ is the focal plane wave complex amplitude after passing through the spatial filter, and $\delta(\mathbf{q})$ is a delta-function. The wavefront sensor output field can be obtained by taking an inverse Fourier transform of (9):

$$\begin{aligned} A_{out}(\mathbf{r}) &= A_{in}(\mathbf{r}) - (1 - e^{i\theta}) \bar{A}, \\ \bar{A} &= \int A_{in}(\mathbf{r}) d^2\mathbf{r}, \end{aligned} \quad (10)$$

where \bar{A} is the spatially averaged input field complex amplitude. For the sake of simplicity, we neglected the 180° rotation of the field performed by the wavefront sensor lens system.

Suppose that the conventional Zernike filter input is $A_{cor}(\mathbf{r}, t) = A_0(\mathbf{r}) \exp\{i[u(\mathbf{r}, t) + \tilde{\phi}(\mathbf{r})]\}$, the corrected beam in the adaptive optic system of Fig. 1. Equation (10) then becomes

$$A_{out}(\mathbf{r}, t) = A_{cor}(\mathbf{r}, t) - (1 - e^{i\theta}) |\bar{A}_0(t)| \exp(i\Delta). \quad (11)$$

For $\theta = \pi/2$, the intensity distribution in the wavefront sensor output plane is then given by

$$I_{out}(\mathbf{r}, t) = I_0(\mathbf{r}) + 2|\bar{A}_0(t)|^2 - 2|\bar{A}_0(t)|A_0(\mathbf{r})\{\cos[u(\mathbf{r}, t) + \tilde{\phi}(\mathbf{r}) - \Delta] - \sin[u(\mathbf{r}, t) + \tilde{\phi}(\mathbf{r}) - \Delta]\}. \quad (12)$$

The output intensity (12) is similar to the typical interference pattern obtained in a conventional interferometer with reference wave – the intensity is a periodic function of the wavefront phase modulation.

2.4. Gradient-flow dynamics and adaptive feedback controller synthesis

Similar to (7), a feedback controller based on the use of the conventional Zernike filter can be represented in the form:

$$\frac{\partial u(\mathbf{r}, t)}{\partial t} = d\nabla^2 u(\mathbf{r}, t) - KI_{out}(\mathbf{r}, t) - \mu[\bar{u}(t) - u_0], \quad (13)$$

where $I_{out}(\mathbf{r}, t)$ is given by equation (12). Comparing equation (12) with the sinusoidal term in equation (6) for the gradient of $J(\mathbf{r}, t)$, we see that equation (12) has three additional terms: $I_0(\mathbf{r}) + 2|\bar{A}_0(t)|^2 - 2A_0(\mathbf{r})|\bar{A}_0(t)|\cos[u(\mathbf{r}, t) + \tilde{\varphi}(\mathbf{r}) - \Delta]$. These additional terms in equation (13) could potentially destroy the gradient-flow dynamics. To evaluate the influence of these “parasitic” terms we simplify the problem by assuming that the input beam intensity distribution is uniform, i.e., $I_0(\mathbf{r}) = I_0 = \text{const}$. In this case the term $I_0 + 2|\bar{A}_0(t)|^2$ is spatially uniform and introduces an additional constant phase shift that has no effect on the dynamics. Indeed, this additional phase shift is automatically compensated due to the penalty term in the cost functional (4) that prevents the average phase from drifting away from some specified value u_0 . A more complicated issue is the impact of the cosine term in (12). Assume the residual (uncompensated) phase distortion $w(\mathbf{r}, t) = u(\mathbf{r}, t) + \tilde{\varphi}(\mathbf{r})$ is small ($|w| \ll 1$ for all \mathbf{r}) and hence the value Δ in (12) approaches zero. In the linear approximation the cosine term in (12) approaches the constant $2A_0|\bar{A}_0|\cos[u(\mathbf{r}, t) + \tilde{\varphi}(\mathbf{r}) - \Delta] \approx 2A_0|\bar{A}_0|$, which does not impact the system dynamics. Therefore, for relatively small-amplitude phase distortions, the adaptive system with the conventional Zernike filter (13) approximates a gradient system. What the numerical and experimental results suggest, however, is that the convergence behavior of the Zernike filter feedback system is actually fairly robust, and extends well beyond the range of small-amplitude phase distortions.

The discrete time version of (13) corresponds to the following iterative wavefront correction algorithm:

$$u^{(n+1)}(\mathbf{r}) = u^{(n)}(\mathbf{r}) + d\nabla^2 u^{(n)}(\mathbf{r}) - KI_{out}^{(n)}(\mathbf{r}) - \mu[\bar{u}^{(n)} - u_0], \quad (14)$$

where the index n defines the iteration number.

2.5. Nonlinear Zernike filter representation

In the nonlinear Zernike filter the phase spatial light modulator (e.g., liquid-crystal light valve) placed in the sensor’s focal plane introduces a phase shift θ dependent on the focal plane intensity distribution $I_F(\mathbf{q})$, i.e., $\theta = \theta(I_F)$. A simple model for the phase SLM is to take the phase shift to be proportional to the focal plane intensity: $\theta = \alpha I_F$, where α is a phase modulation coefficient. If the Strehl ratio is sufficiently large, enough of the intensity is in the zero-order spectral component that the nonlinear Zernike filter is well-approximated by a conventional Zernike filter model (with central spectral component phase shift proportional to its intensity). The analysis presented above for $\theta = \pi/2$ also holds for $0 < \theta < \pi$, with some additional factors involving $\cos\theta$ and $\sin\theta$ appearing, and the fact that θ changes with time (as the Strehl ratio changes) also does not upset the analysis. To keep the analytical feedback system model manageable, we treat the nonlinear Zernike filter as a conventional Zernike filter with a time-varying zero-order spectral component phase shift. Some of the effects of spectral components besides the zero-order component being phase shifted have also been analyzed.¹⁶

3. NONLINEAR ZERNIKE FILTER FEEDBACK SYSTEM EXPERIMENTAL RESULTS

3.1. Liquid crystal light valve phase modulator for nonlinear Zernike filter

The key element of the nonlinear Zernike filter is an optically addressed phase spatial light modulator.¹⁷ For the nonlinear Zernike filter used in the experiments described here, a specially designed optically addressed liquid crystal light valve was manufactured. The schematic of the LCLV is shown in Fig. 3. The LCLV is based on parallel-aligned nematic LC with high refractive index anisotropy, and a transmissive, highly photo-sensitive, amorphous hydrogenated silicon

carbide α -SiC:H film with diameter 12 mm and thickness near 1 μm . The photo-conductive film was fabricated by PeterLab Inc. (St. Petersburg, Russia). The nematic LC has low viscosity and an effective birefringence $\Delta n = 0.27$ for $\lambda = 0.514 \mu\text{m}$. The thickness of the LC layer is 5.2 μm .

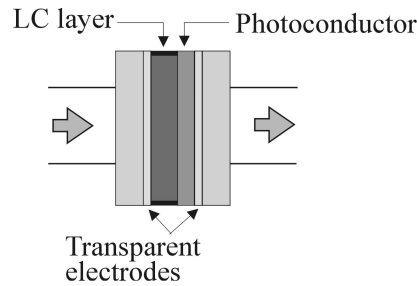


Fig. 3. Schematic of the liquid-crystal light valve

The intensity distribution on the LCLV photo-conductor film is transferred to an appropriate spatial distribution of the voltage applied to the LC layer. This results in a corresponding spatially distributed change of the LC molecule orientation from planar to homeotropic.^{18,19} The LCLV is transmissive and operates in a pure phase-modulation mode when linearly polarized light with polarization axis parallel to the LC molecule director passes through the LC layer. The phase change $\theta = (2\pi/\lambda) d\Delta n$ introduced by the LCLV is determined by the LC layer thickness d and wavelength λ , and the effective LC birefringence Δn , dependent on such characteristics as the LC type, applied voltage, wavelength of the incident light, and temperature. Because the light-generated voltage pattern on the LC layer is dependent on the intensity distribution on the photo-conductor film, Δn is a function of both the intensity I_F on the LCLV photo-conductor layer and the amplitude of sine wave voltage V applied to the LCLV electrodes. Correspondingly, the phase shift $\theta = (2\pi/\lambda) d\Delta n(I_F, V, \lambda)$ introduced by the LCLV is also dependent on the intensity I_F , applied voltage V , and wavelength λ .

3.2. Feedback system incorporating the nonlinear Zernike filter

A schematic diagram of the experimental setup is shown in Fig. 4.¹³ The laser beam from the He-Ne laser (12 mm diameter) entered the system and sequentially passed through two HEX127 multi-electrode liquid crystal spatial phase modulators (SLM_1 and SLM_2) from Meadowlark Optics. The HEX127 LC phase modulators contain 127 independently controllable, hexagonal LC cells. SLM_1 was used to correct static random phase distortions introduced by the second phase modulator SLM_2 . This phase SLM was controlled using a computer (PC_2). The amplitude of the introduced phase distortions was in the range of $[0, 3\pi \text{ rad.}]$.

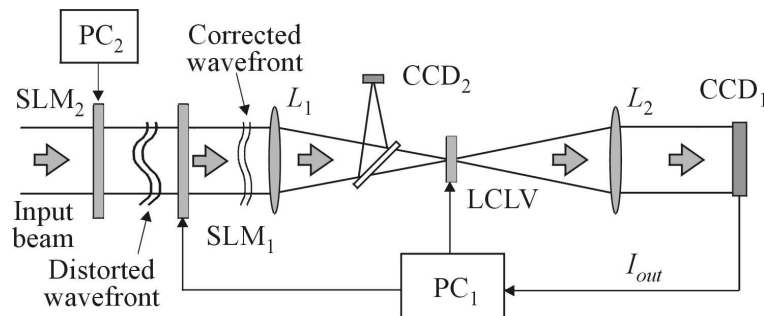


Fig. 4. Schematic of experimental setup for adaptive wavefront phase distortion compensation using nonlinear Zernike filter.

The phase-distorted wave entered the nonlinear Zernike filter, which contained two identical lenses (L_1 and L_2) with 300mm focal lengths, and the optically addressed LC phase modulator (LCLV). Output intensity from the nonlinear Zernike filter was captured by the camera (CCD_1) and sent to a computer (PC_1), which implemented the feedback algorithm (14) with

no diffusion term. The intensity distribution of the corrected beam in the focal plane of lens L_1 was registered by a camera (CCD₂). To improve the contrast of the nonlinear Zernike sensor output, the AC bias voltage V applied to the LCLV was controlled electronically, thus providing adaptive changing of the phase modulation coefficient α during the adaptation process. The voltage amplitude V was dependent on the computed aperture-averaged variance of the Zernike filter output intensity distribution. This applied voltage amplitude V was decreased from 6 volts at the beginning of adaptation to 2.4 volts at the end.

Fig. 5 shows experimental results of adaptive wavefront phase distortion correction in the direct-control system with the nonlinear Zernike filter.¹³ Before adaptation random voltages were applied to the phase modulator (SLM₂). For independent analysis of wavefront aberrations during the adaptation process we used a Mach-Zender interferometer (not shown in Fig. 4). An interference pattern corresponding to an initially phase-distorted wave is shown in Fig. 5a. The initial random phase modulation resulted in the random intensity distribution pattern in the lens L_1 focal plane, as seen in Fig. 5b. Adaptation resulted in compensation of the introduced random phase distortion, except for wavefront tilts. The interference pattern of the wavefront after 34 iterations of adaptive correction is shown in Fig. 5c, and the corresponding intensity distribution in the lens focal plane is shown in Fig. 5d. A factor of eight improvement in the Strehl ratio was obtained for the case shown in Fig. 5. Each iteration took about two seconds, with most of the delay used to ensure that the phase-correcting SLM was fully updated between iterations.

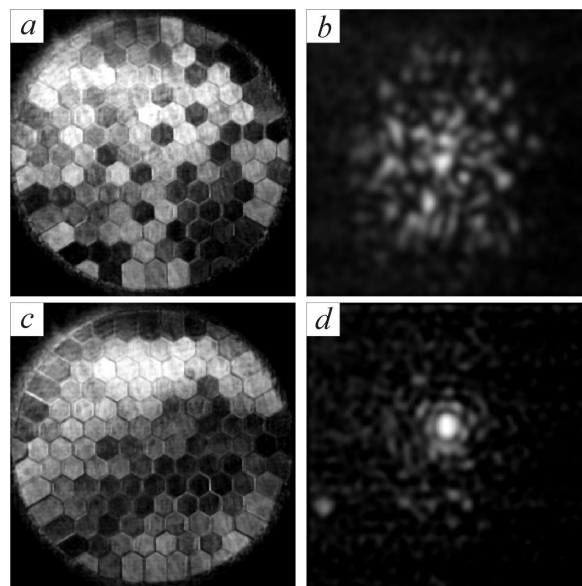


Fig. 5. Experimental results for adaptive system with nonlinear Zernike wavefront sensor: (a) interference pattern for the aberrated beam, and (b) corresponding intensity distribution in the lens focal plane; (c) and (d) are the same but for the corrected wavefront.

One of the behaviors observed both experimentally and in simulation for the nonlinear Zernike filter is a winner-take-all behavior in the Fourier domain. Fig. 6 shows snapshots of the Fourier spectrum during adaptation for one trial run of the experimental nonlinear Zernike filter feedback system. After 10 iterations, the spectral power has coalesced into several peak-intensity components; after 20 iterations, most of the power is concentrated in two components; and after 30 iterations, the power is seen to be concentrated in a single spectral component. This winner-take-all behavior is important for the nonlinear Zernike filter, because it means wavefront correction is possible even when the zero-order spectral component of the aberrated input beam does not dominate the other spectral components. For the gradient system sharing the same linearized dynamics as the nonlinear Zernike filter feedback system, this winner-take-all behavior can be studied analytically.¹⁶

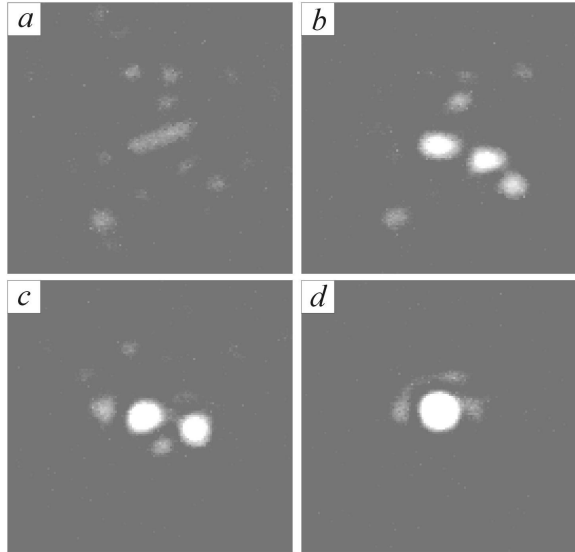


Fig. 6. Winner-take-all behavior in the Fourier domain for the adaptive system with nonlinear Zernike filter: focal plane intensity distribution (a) initially; (b) after 10 iterations, (c) after 20 iterations, and (d) after 30 iterations

4. RELATED FEEDBACK SYSTEMS USING ADVANCED PHASE-CONTRAST SENSORS

The primary advantage of the LCLV-based nonlinear Zernike filter is ease of implementation: the only electronics required for the wavefront sensor are to provide the bias voltage for the transparent electrodes. However, better performance can potentially be obtained by using an electronically-controlled phase SLM in the focal plane instead of the LCLV. We refer to these systems as opto-electronic Zernike filters. From measurement of the focal plane intensity distribution (e.g., using a photodetector array collocated with the phase SLM, as shown in Fig. 7), a phase-shift distribution could be computed for the focal-plane phase SLM which could do a better job of approximating an ideal Zernike phase plate than the LCLV. For example, the opto-electronic Zernike filter could be designed to supply a phase-shift of $\pi/2$ for whichever spectral component had the greatest intensity.

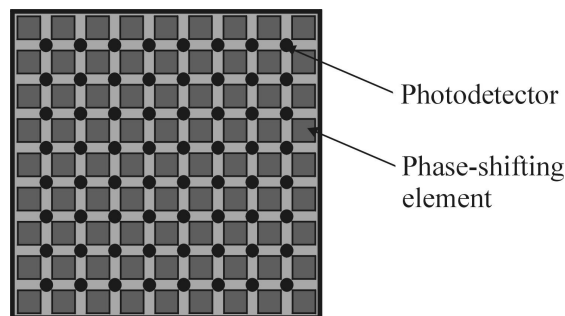


Fig. 7. Schematic of a phase SLM for an opto-electronic Zernike filter.

Even better performance can potentially be achieved using a “differential” Zernike filter, in which the wavefront sensor output is obtained by differencing the intensity distributions corresponding to zero-order spectral component phase shifts of $\pi/2$ and $-\pi/2$. If input beam wavefront tilts are removed prior to the wavefront sensor, the differential Zernike filter can be implemented using a focal-plane phase-shifting device with a single pixel, as shown in Fig. 8. However, the opto-electronic phase SLM shown in Fig. 7 could also be used. The advantage of the differential Zernike filter is that the gradient dynamics of equation (7) can be implemented exactly. Therefore, the convergence behavior of the differential Zernike filter is global, while for the nonlinear Zernike filter, only a linearized stability analysis is available. Furthermore, the convergence property of the differential Zernike filter is retained even in the presence of strong intensity scintillations.¹³

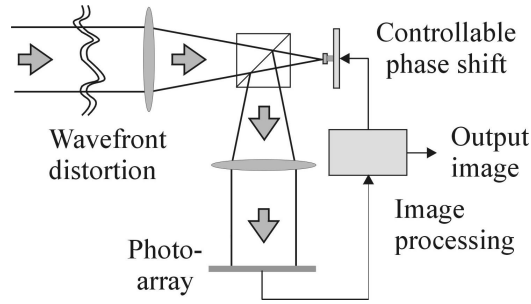


Fig. 8. Differential Zernike filter wavefront sensor.

5. STATISTICAL ANALYSIS OF ZERNIKE-FILTER-BASED ADAPTIVE SYSTEMS

Performance of the adaptive system with a conventional, nonlinear, and opto-electronic Zernike filter was analyzed numerically using phase distortions with the Andrews model for atmospheric turbulence-induced phase fluctuation power spectra.²⁰ Simulations were performed for an input wave with a uniform intensity distribution and random phase aberration $\varphi(\mathbf{r})$ applied inside the aperture D . The strength of the input phase aberration was characterized by the standard deviation of the phase fluctuations averaged over the aperture $\sigma_\varphi = [S^{-1} \int \tilde{\varphi}^2(\mathbf{r}) d^2\mathbf{r}]^{1/2}$ and by the Strehl ratio St . The amplitude of the introduced phase distortions was varied by changing the value of the Fried parameter r_0 .²¹ For each fixed value r_0 , 200 phase screens were generated. A fixed number of iterations N corresponding to the discrete-time wavefront control algorithm (14) were performed for each realization of the phase-distorted input field. Adaptive system performance was evaluated using a Strehl ratio value of St_N achieved after N iterations. For fixed Fried radius r_0 the iteration process was repeated for each of 200 phase distortion realizations, and the obtained values St_N were averaged. The averaged Strehl ratios $\langle St_N \rangle$ are presented in Figs. 9 and 10 as functions of the ensemble-averaged standard deviation of the phase fluctuation $\sigma_{in} = \langle \sigma_\varphi \rangle$ for different iteration numbers. In all calculations, the parameters we used were $d=0$, $K=0.75$, $\mu=1$ and $u_0=0$.

In the nonlinear Zernike filter the phase spatial light modulator placed in the sensor's focal plane introduces a phase shift θ dependent on the focal plane intensity distribution $I_F(\mathbf{q})$, i.e., $\theta = \theta(I_F)$. In numerical simulations we considered a simple model for the phase SLM with phase shift proportional to the focal plane intensity: $\theta = \alpha I_F$, where α is a phase modulation coefficient. Results of the numerical analysis for the corresponding adaptive system are presented in Fig. 9 for different phase modulation coefficients α . The adaptive feedback system based on the nonlinear Zernike filter is capable of compensating phase distortions with an amplitude in the range of $\sigma_{in} \approx 1.2$ rad. Increasing α up to $\alpha \approx \pi/I_F^0$ leads to some extension of this range, but causes performance degradation in the region $0.5 < \sigma_{in} \leq 1.2$ rad: the Strehl ratio is near 0.95 for $\alpha = \pi/I_F^0$ and near 0.98 for $\alpha = 0.5\pi/I_F^0$ (compare curves 3 and 4 in Fig. 9). This suggests a control strategy with coefficients α that can be changed during the adaptation process dependent upon the residual phase amplitude. In the region of large-amplitude phase distortions ($\sigma_{in} > 2.0$ rad.) the value of α should be near π/I_F^0 , or even larger; during the adaptation process it should be decreased down to the value $\alpha = 0.5\pi/I_F^0$. (This adaptive adjustment of the phase modulation coefficients was used in the experiments described above.)

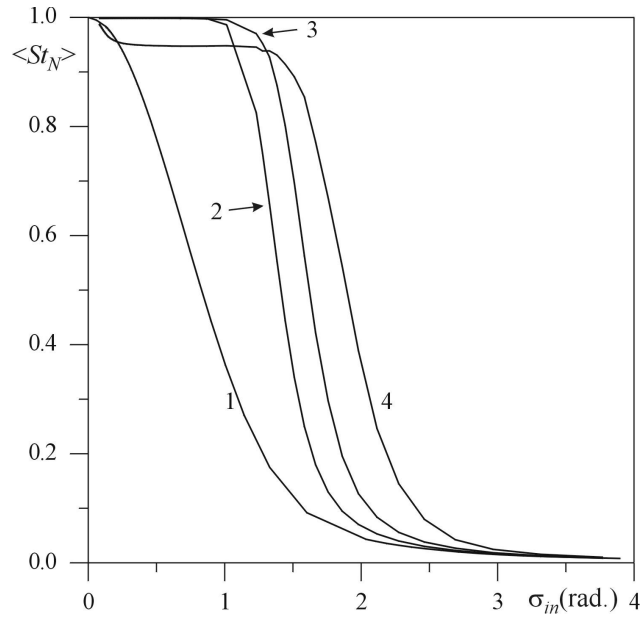


Fig. 9. Simulation results for 10 iterations of the adaptive system with the nonlinear Zernike filter for different phase modulation coefficients α : (1) $\alpha = 0$ (no adaptation); (2) $\alpha = 0.25\pi / I_F^0$; (3) $0.5\pi / I_F^0$; and (4) $\alpha = 1.0\pi / I_F^0$.

To put the numerical results for the nonlinear Zernike filter in perspective, Fig. 10. shows corresponding results for conventional, opto-electronic, and differential Zernike filter feedback systems. The opto-electronic Zernike filter model used in the calculations corresponded to a $\pi/2$ phase shift for the spectral component having the highest intensity level. In the conventional Zernike filter wavefront sensor model, a phase shift of $\pi/2$ was applied to the zero spectral component. (Although it appears from Figs. 9 and 10 that the conventional Zernike filter system out-performs the nonlinear Zernike filter system, these data conceal the fact that for large enough initial wavefront tilts, a practical implementation of the conventional Zernike filter will not produce a large enough signal-to-noise ratio for adaptation to begin.)

Figs. 9 and 10 indicate that the differential Zernike filter feedback system is the best-performing system, and the opto-electronic and nonlinear Zernike filter feedback systems can be considered as trading off performance for ease of implementation. When input beam intensity scintillations are present in addition to phase distortion, the same tradeoff still applies, but the performance differences among the nonlinear, opto-electronic, and differential Zernike filters are more dramatic.¹³

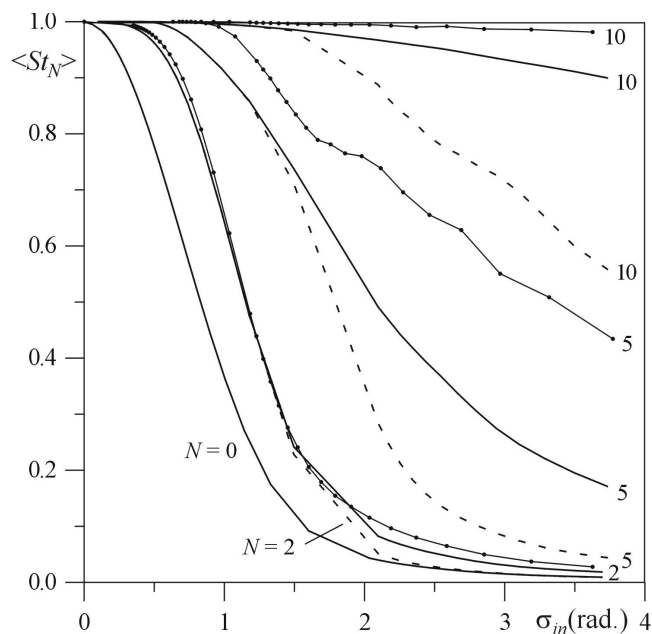


Fig. 10. Averaged Strehl ratio achieved after N iterations of the adaptation process vs. input phase standard deviation for the following adaptive system configurations: conventional (dashed lines); opto-electronic (solid lines); differential (solid lines with dots). Numbers near curves correspond to the number of iterations N , the curve with $N=0$ corresponds to $K=0$ (no adaptation).

6. CONCLUSION

The direct-control adaptive optics technique presented here offers an attractive alternative to both the conventional phase-conjugation adaptive system²² and adaptive optics based on model-free optimization techniques.²³ In comparison with the conventional phase-conjugation approach, the direct-control adaptive optics paradigm doesn't require wavefront reconstruction and can be used for high-resolution adaptive wavefront control. Similar to model-free gradient descent optimization techniques, the direct-control approach is also based on gradient descent optimization, but considers gradient-flow optimization. This results in dramatic improvement in the adaptation process convergence speed when compared with model-free optimization adaptive optics. The key element of the direct-control adaptive optical system is the wavefront sensor, which is not used for wavefront reconstruction as in conventional adaptive optics, but rather for measuring the gradient of the optimized cost function (in our case the gradient of the Strehl ratio). It is shown that wavefront sensors based on advanced phase-contrast techniques can provide information about the cost function gradient that can be used for synthesis of the gradient-flow feedback controller. The best adaptive system performance can be achieved using a differential Zernike filter, as its output is proportional to the Strehl ratio gradient. The nonlinear Zernike filter shares the same linearized behavior as the differential Zernike filter, but for large phase distortions the non-gradient terms that appear in the nonlinear Zernike filter feedback system adversely impact system performance.

A practical implementation of the direct-control adaptive system requires both the development of advanced phase-contrast wavefront sensors and a very large scale (VLSI) parallel computational controller to interface the wavefront sensor and wavefront shaping device. Analysis and numerical work indicates that the LCLV-based nonlinear Zernike filter can be out-performed in an adaptive system by the opto-electronic or differential Zernike filters. Nevertheless, the LCLV-based nonlinear Zernike filter is much more readily implemented for proof-of-concept experiments.

ACKNOWLEDGEMENTS

We thank J. C. Ricklin for technical and editorial comments. Work was performed at the Army Research Laboratory's Intelligent Optics Lab in Adelphi, Maryland. This work was supported in part by grants from the Army Research Office under the ODDR&E MURI97 Program Grant No. DAAG55-97-1-0114 to the Center for Dynamics and Control of Smart Structures (through Harvard University).

REFERENCES

1. V. P. Sivokon and M. A. Vorontsov, "High-resolution adaptive phase distortion suppression based solely on intensity information," *J. Opt. Soc. Am. A*, **15**, 1, 234-247 (1998).
2. M. A. Vorontsov, "High-resolution adaptive phase distortion compensation using a diffractive-feedback system: experimental results," *J. Opt. Soc. Am. A*, **16**, 2567-2573 (1999).
3. R.A. Muller and A. Buffington, "Real-time correction of atmospherically degraded telescope images through image sharpening," *J. Opt. Soc. Am.*, **64**, 1200-1210 (1974).
4. T.R. O'Meara, "The multi-dither principle in adaptive optics," *J. Opt. Soc. Am.*, **67**, 306-315 (1977).
5. M. A. Vorontsov and V. I. Shmalhauzen, *Principles of Adaptive Optics*, Nauka, Moscow (1985).
6. J. C. Spall, "A Stochastic approximation technique for generating Maximum Likelihood Parameter estimates," *Proceedings of the American Control Conference*, 1161-1167 (1987).
7. G. Cauwenberghs, "A Fast Stochastic Error-Descent Algorithm for Supervised Learning and Optimization," in S .J. Hanson, J. D. Cowan and C. L. Giles eds., *Advances in Neural Information Processing Systems*, San Mateo, CA: Morgan; Kaufman, **5**, 244-251 (1993).
8. M. A. Vorontsov, G. W. Carhart and J. C. Ricklin, "Adaptive phase-distortion correction based on parallel gradient-descent optimization," *Opt. Lett.*, **22**, 907-909 (1997).
9. M. A. Vorontsov, and V. P. Sivokon, "Stochastic parallel gradient descent technique for high-resolution wavefront phase distortion correction," *J. Opt. Soc. Am. A*, **15**, 2745-2758 (1998).
10. *Geometry-driven Diffusion in Computer Vision*, Bart M. ter Haar Romey, ed., Kluwer Academic Publishers, Dordrecht (1994).
11. *IEEE Transactions on Image Processing*, (Special issue on partial differential equations and geometry-driven diffusion in image processing and analysis), **7**, No. 3, March (1998).
12. M. A. Vorontsov, "Parallel image processing based on an evolution equation with anisotropic gain: integrated opto-electronic architectures," *J. Opt. Soc. Am. A*, **16**(7), 1623-1637 (1999).
13. E. W. Justh, M. A. Vorontsov, G. W. Carhart, L. Beresnev, and P. S. Krishnaprasad, "Adaptive Optics with Advanced Phase-Contrast Techniques: Part II. High-Resolution Wavefront Control," submitted to *J. Opt. Soc. Am. A*, 2000.
14. F. Zernike, "How I Discovered Phase Contrast," *Science*, **121**, 345-349 (1955).
15. J.W. Goodman, "*Introduction to Fourier Optics*," McGraw-Hill (1996).
16. E. W. Justh, P. S. Krishnaprasad, and M. A. Vorontsov, "Nonlinear Analysis of a High-Resolution Optical Wavefront Control System," submitted to the IEEE Conference on Decision and Control, 2000.
17. M. A. Vorontsov, E. W. Justh, and L. Beresnev, "Adaptive Optics with Advanced Phase-Contrast Techniques: Part I. High-Resolution Wavefront Sensing," submitted to *J. Opt. Soc. Am. A*, 2000.
18. U. Efron, Ed., *Spatial Light Modulator Technology: Materials, Devices, and Applications*, Marcel Dekker Press, New York (1995).
19. V.G. Chigrinov, *Liquid Crystal Devices: Physics and Applications*, Artech House, Boston (1999).
20. L. C. Andrews, "An analytic model for the refractive index power spectrum and its application to optical scintillations in the atmosphere," *J. Mod. Opt.*, **39**, 1849-1853 (1992).
21. D. L. Fried, "Statistics of a Geometric Representation of Wavefront Distortion," *J. Opt. Soc. Am.*, **55**, 1427-1435 (1965).
22. C. A. Primmerman, T. R. Price, R. A. Humphreys, B. G. Zollars, H. T. Barclay, and J. Herrmann, "Atmospheric-compensation experiments in strong-scintillation conditions," *Appl. Opt.*, **34**, 2081-2088 (1995).
23. *Adaptive Optics in Astronomy*, F. Roddier, ed., 91- 130, Cambridge University Press (1999).
23. M. A. Vorontsov, G. W. Carhart, M. Cohen and G. Cauwenberghs, "Adaptive optics based on analog parallel stochastic optimization: analysis and experimental demonstration," *J. Opt. Soc. Am. A* (to appear).